Optimization of operational parameters in the mechanochemical regeneration of sodium borohydride ($NaBH_4$)

Garrido Nuñez, Santiago; Schott, Dingena L.; Padding, Johan T.

DOI
10.1016/j.ijhydene.2024.11.360

Publication date
2025

Document Version
Final published version

Published in
International Journal of Hydrogen Energy

International Journal of Hydrogen Energy 97 (2025) 640–648

Contents lists available at ScienceDirect

International Journal of Hydrogen Energy

journal homepage: www.elsevier.com/locate/he

Optimization of operational parameters in the mechanochemical regeneration of sodium borohydride ($NaBH_4$)☆

Santiago Garrido Nuñez [a,*], Dingena L. Schott [b], Johan T. Padding [a]

[a] Department of Process and Energy, Delft University of Technology, Leeghwaterstraat 39, Delft, 2628 CB, The Netherlands
[b] Department of Maritime and Transport Technology, Delft University of Technology, Mekelweg 2, Delft, 2628 CD, The Netherlands

ARTICLE INFO

Keywords:
Ball milling
Hydrogen
Sodium borohydride
Mechanochemistry

ABSTRACT

In this study we investigate the mechanochemical regeneration of sodium borohydride ($NaBH_4$) from a system comprising hydrated sodium metaborate ($NaBO_2 \cdot 4\,H_2O$) and magnesium hydride (MgH_2). We explore the individual and joint impact of key operational parameters (rotational speed, milling time, ball-to-powder ratio (BPR), and molar ratio) on the regeneration yield. Furthermore, a method for quantifying chemical conversion is introduced relying only on water and thus, offering environmental benefits. This approach additionally facilitates the production and storage of a "ready-to-use" $NaBH_4$ solution with minimal losses at room temperature. Notably, a yield of 90% is achieved, with a 20% reduction in rotational speed compared to prior literature. This research contributes to sustainable hydrogen storage and presents practical advancements in mechanochemical processes.

1. Introduction

The ongoing transition to low-carbon and no-carbon energy systems has incentivized the creation of many green power generation solutions that have the potential to sustain our energetic needs. This transition faces a great challenge in finding an effective and efficient energy carrier that can keep up with the demands of high-energy industries and applications such as maritime transport [1,2]. One of the alternatives to mitigate fossil fuel dependency is hydrogen, a clean energy carrier with zero emissions. However, hydrogen storage and transportation in pure gaseous or liquid form is challenging due to high-pressure or low-temperature working conditions [3,4].

A potential solution involves using solid hydrogen carriers, which enable the storage of hydrogen at ambient temperature and pressure conditions. Sodium borohydride ($NaBH_4$) has a high theoretical gravimetric hydrogen storage capacity (10.92 wt%) and thus, is a promising solid hydrogen carrier [5]. Hydrogen can be released via the hydrolysis of $NaBH_4$ (Eq. (1)) with dry or hydrated sodium metaborate ($NaBO_2 \cdot xH_2O$) as byproduct, typically referred to as spent fuel. Therefore, the regeneration of $NaBH_4$ from the spent fuel is critical for considering it a viable contributor to the energy transition since it would allow its usage in a circular, cheap and sustainable manner [6,7].

$$NaBH_4 + (2 + x)H_2O \rightarrow NaBO_2 \cdot xH_2O + 4\,H_2 \quad (1)$$

where x is the level of hydration.

Mechanochemical, electrochemical, and thermochemical methods have been reported for regenerating $NaBH_4$ [6,8,9]. Thermochemical processes require high pressure and temperature conditions, while electrochemical methods tend to be inefficient and can produce toxic or harmful byproducts that have a negative impact on the environment. Mechanochemical methods, in contrast, are appealing and environmentally friendly options because they function without the need of an electrolyte solution and can be performed at room temperature and pressure conditions [6].

Within a mechanochemical process, the mechanical action of the system induces the breakage of primary bonds giving rise to surface reconstruction and chemical reactions among the surrounding media as milling balls collide [10]. For the chemical reaction to take place, a sufficiently large contact area and contact time must be involved in the process. Otherwise, the reactants may not have sufficient interplay.

In the specific case of $NaBH_4$, its mechanochemical regeneration has been reported to be viable in high-energy mills [11–17]. A summary of the highest yield obtained in different studies is presented in Table 1.

The results presented in Table 1 are based on the following five distinct chemical processes.

$$NaBO_2 + 2\,MgH_2 \rightarrow NaBH_4 + 2\,MgO \quad (2)$$

☆ This project has received funding from the Ministry of Economic Affairs and Climate Policy, RDM regulation, carried out by The Netherlands Enterprise Agency (RvO).

* Corresponding author.
E-mail address: s.garridonunez@tudelft.nl (G. Garrido Nuñez).

https://doi.org/10.1016/j.ijhydene.2024.11.360
Received 23 September 2024; Received in revised form 20 November 2024; Accepted 21 November 2024
Available online 4 December 2024

Table 1
Reported results of the mechanochemical regeneration of $NaBH_4$ in literature.

Metaborate	2nd reactant	Reported yield (%)	Year	Ref.
$NaBO_2$	MgH_2	76	2009	[11]
$NaBO_2$	MgH_2	71	2009	[12]
$NaBO_2$	MgH_2	74	2011	[13]
$NaBO_2$	MgH_2	89	2017	[14]
$NaBO_2 \cdot 2\,H_2O$	Mg	68	2017	[15]
$NaBO_2 \cdot 2\,H_2O$	MgH_2	90	2017	[16]
$NaBO_2 \cdot 4\,H_2O$	MgH_2	88	2017	[16]
$NaBO_2 \cdot 2\,H_2O$	Mg_2Si	78	2017	[17]

$$NaBO_2 \cdot 2\,H_2O + 4\,Mg \rightarrow NaBH_4 + 4\,MgO \quad (3)$$

$$NaBO_2 \cdot 2\,H_2O + 4\,MgH_2 \rightarrow NaBH_4 + 4\,MgO + 4\,H_2 \quad (4)$$

$$NaBO_2 \cdot 4\,H_2O + 6\,MgH_2 \rightarrow NaBH_4 + 6\,MgO + 8\,H_2 \quad (5)$$

$$NaBO_2 \cdot 2\,H_2O + 2\,Mg_2Si \rightarrow NaBH_4 + 4\,MgO + 2\,Si \quad (6)$$

It can be noticed that significantly different yields have been achieved using the same reactants. This variation is due to differences in the working conditions of the ball mills used (e.g., rotational speed, fill ratio, ball size, jar shape, ball mill motion or ball-to-powder ratio (BPR)). These parameters fundamentally affect the mechanical action within the milling jar. It is important to emphasize that mechanical conditions depend on the specific ball mill and the collisions occurring inside the jar. Therefore, simply replicating operational conditions does not guarantee the same chemical yield unless the same mechanical action inside the jar is ensured. The process parameters reported in the studies shown in Table 1 are as follows.

The results presented in Tables 1 and 2 highlight the significant potential of mechanochemistry in facilitating the regeneration of $NaBH_4$, which serves as a motivation for this study. However, it is worth noting that many authors have omitted crucial details for the complete characterization of their experimental setup, thereby hindering reproducibility.

Moreover, most authors typically investigate the impact of only one or two operational variables at a time while holding the remaining variables constant. For instance, Hsueh et al. [11] simultaneously varied milling time and molar ratio while keeping rotational speed and BPR constant. In contrast, Lang et al. [14], Çakanyildirim et al. [13] and Chen et al. [16] independently varied milling time and molar ratio while maintaining the remaining variables fixed. Kong et al. [12] independently varied milling time, molar ratio, and ball-to-powder ratio (BPR) while keeping the rest of variables constant. Notably, the work of Ouyang et al. [15] stands out as they studied the simultaneous effects of varying milling time, molar ratio, and BPR. However, their maximum yield fell short compared to other studies. Finally, Zhong et al. [17] also analyzed the combined influence of milling time and molar ratio while keeping the other variables constant.

It is understandable why authors have decided to follow this approach. The number of experiments increases exponentially as more parameters are varied simultaneously and the effect can be even more dramatic depending on the amount of levels or values assigned to these variables. However, it is crucial to recognize that all these operational variables impact the chemical yield. To provide a simple example, while it may be intuitive to fix the rotational speed of the milling jar at a constant value that can deliver sufficient kinetic energy to the milling balls, one needs to realize that it also directly influences the collision frequency. This affects the amount of events (effective collisions) that ultimately enable the chemical reaction to take place. If one then decreases the BPR to include more powder, the chemical yield will inevitably be reduced as the collisions available to treat the total amount of powder have effectively changed. In this situation, one could arguably compensate by increasing the rotational speed or the milling time. Needless to say, the molar ratio also plays a key role as it impacts the amount of effective collisions where both reactants are crushed together. This chain of events can be visualized in Fig. 1.

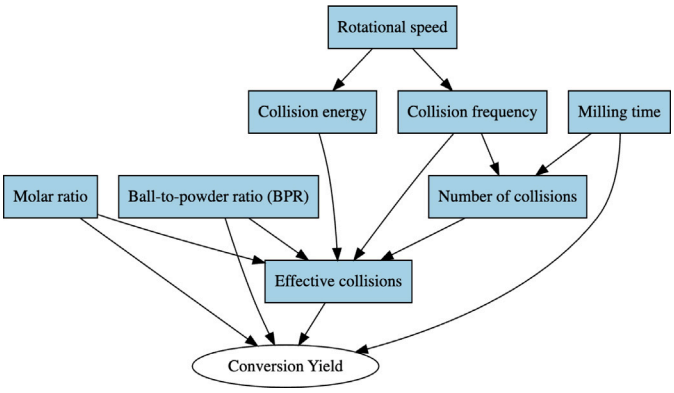

Fig. 1. Graphical model of variable interplay.

As a result of the previous observations and the insights gained by the studies shown in Table 2, this study aims to optimize and enhance the understanding of the mechanochemical regeneration of $NaBH_4$ by investigating the individual and joint effects of milling time, BPR, molar ratio, and rotational speed on the chemical yield. Consistent with our prior investigations, we maintain a fill ratio of 10%, achieved with twenty-four 10 mm milling balls. In our milling machine, this fill ratio achieves an optimal balance between normal and tangential dissipation during collisions, while the size of milling balls primarily affects the distribution of energy dissipation per rotation cycle [18]. Furthermore, we opt for the chemical pathway consisting of $NaBO_2 \cdot 4\,H_2O$ and MgH_2 (Eq. (5)) as this reaction has shown to enable high conversion yields and it eliminates the need to dedicate additional energy drying the sodium metaborate or to artificially create a hydrogen atmosphere inside the milling jar [16].

2. Materials and methodology

2.1. High-energy ball milling

The Emax high-energy ball mill is a device produced and distributed by the German company Retsch. It offers a novel approach to ball milling by combining high friction and impact results with a temperature control system allowing for controlled grinding. The system was set up to allow a maximum temperature of 50 °C. The machine can allocate proprietary grinding jars with 125 ml of volume that follow a circular motion with a rotational speed n up to 2000 revolutions per minute (corresponding to an angular frequency of $\omega = 2\pi n/60 = 209$ rad/s) with an amplitude (radius) A of 1.7 cm, see Fig. 2.

Stainless steel milling balls with diameter of 10 mm (1.4034 G100 DIN 5401), purchased from Kugel Pompel, were utilized in all experiments.

2.2. Chemicals

Hydrated sodium metaborate ($NaBO_2 \cdot 4\,H_2O$) (≥99%) was purchased from Sigma-Aldrich. Magnesium hydride (MgH_2) (≥99.9%, ≤50 μm) was purchased from Nanoshel. All chemicals were used as received. Additionally, all samples for ball milling were prepared in a glove box under an Argon environment where concentrations of oxygen and water were below 0.1 ppm.

Table 2
Process parameters reported for the mechanochemical regeneration of $NaBH_4$. Parameters that have not been specified are indicated by "–".

Reference	[11]	[12]	[13]	[14]	[15]	[16]	[17]
Metaborate	$NaBO_2$	$NaBO_2$	$NaBO_2$	$NaBO_2$	$NaBO_2 \cdot 2\,H_2O$	$NaBO_2 \cdot 4\,H_2O$	$NaBO_2 \cdot 2\,H_2O$
2nd reactant	MgH_2 (98%)	MgH_2 (79.3%)	MgH_2 (99%)	MgH_2 (95%)	Mg (99.8%)	MgH_2 (99%)	Mg_2Si (99.5%)
Mass of metaborate [g]	0.66	–	0.86	–	0.43	0.44	0.31
Mass of 2nd reactant [g]	0.26	–	0.89	–	0.57	0.56	0.69
Total mass of reactants [g]	0.92	–	1.75	–	1	1	1
Molar ratio	2.8	2	2.6	2.7	5.5	5	3
Rotational speed [rpm]	1080	–	1450	–	1200	1200	1000
Milling time [h]	6	2	12	12	10	15	20
Volume of jar [ml]	65	–	45	–	80	80	–
Diameter of balls [mm]	13	–	10 and 4	–	–	–	–
Number of balls	4	–	2 and 3	–	–	–	–
Volume of balls in the reactor [%]	7	–	2.5	–	8	8	–
Ball-to-powder ratio [kg:kg]	39	50	10	50	50	50	50
Ball mill	SPEX CertiPrep 8000-series (shaker mill)	QM-3A (vibrating mill)	CertiPrep 8000M (shaker mill)	QM-3A (vibrating mill)	QM-3C (shaker mill)	QM-3C (shaker mill)	QM-3C (shaker mill)
Milling material	Steel	–	–	–	Steel	Steel	–
Yield [%]	76	71	70	89	68	90	78

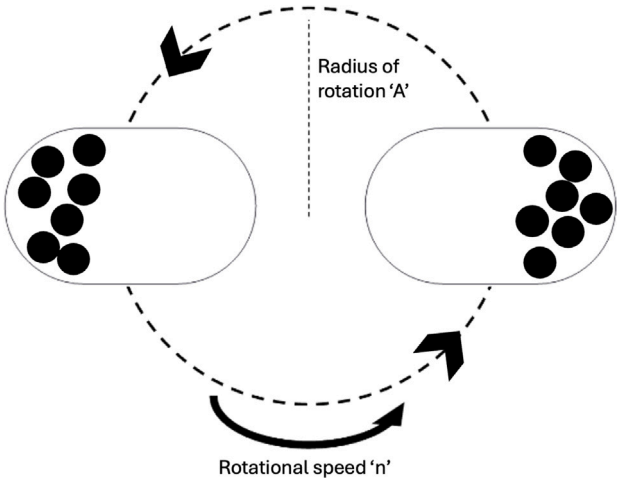

Fig. 2. Schematic of jar movement.

2.3. Equipment cleaning

To preserve similar conditions for all our experimental cases, after every 3 experiments, the jars were cleaned and the milling balls were replaced with new ones. We have found that cleaning the jar by milling 1 g of silica sand and adding 10 ml of isopropyl alcohol provides excellent results in removing any leftover contamination. The typical duration for the cleaning process was 6 min. Upon finishing, the jar is then rinsed thoroughly with pure water, air-blasted with compressed air, and left to dry open to the ambient.

2.4. Quantification of conversion yield

In the studies presented in Table 1, the standard approach for quantifying the regenerated $NaBH_4$ via mechanochemistry involves utilizing ethylenediamine (EDA). EDA possesses a distinct advantage as it selectively dissolves $NaBH_4$ while leaving the remaining reactants intact, facilitating an efficient separation process through subsequent filtering and sublimation. However, EDA poses risks such as corrosion, toxicity, and health hazards. Hence, we propose a cheaper, safer and more environmentally friendly method to assess the conversion yield, leveraging any unconverted MgH_2 in the process.

After the ball milling process is completed, the jar is opened to the atmosphere and pure water is added. This promptly initiates the self-hydrolysis of unconverted MgH_2, elevating the solution's pH above 11 within seconds [19]. Hydrogen is released from this hydrolysis until dense passivation layers of magnesium hydroxide form over unconverted magnesium hydride [20–22]. While hydrogen released in this step is carefully disposed of, it could also be utilized to enhance overall hydrogen release in the system. The half-life of this solution, representing the time for half of the $NaBH_4$ solution to decompose, can be calculated as 10.2 h at pH = 11 and temperature of 25 °C, based on the work by Kreevoy and Jacobson (Eq. (7)) [23]. Thus, a significant advantage of the rapid pH increase is the immediate inhibition of $NaBH_4$ self-hydrolysis, minimizing hydrogen losses for quantification purposes [24,25].

$$\log_{10}(t_{1/2}) = \mathrm{pH} - (0.034T - 1.92) \tag{7}$$

where $t_{1/2}$ represents the half time in minutes and T is the temperature in Kelvin.

After the stabilization of MgH_2 by self-hydrolysis, the jar is sealed again with a lid featuring a unidirectional flow valve and connected to a gas-collection over water system. Subsequently, Ru-based catalysts are introduced into the solution within the jar, and the temperature is raised to 80 °C. This catalyst specifically assists the hydrolysis of $NaBH_4$, as the hydrolysis of MgH_2 remains relatively inactive at temperatures below 200 °C [26–30] for non-catalized mixtures and 146 °C for catalyzed mixtures [31,32]. Moreover, Ru-based catalysts are favored for $NaBH_4$ hydrolysis due to their high hydrogen generation rates, durability, and efficient catalytic activity, particularly in comparison to other metals like Pt or Pd. These catalysts are well-suited

for hydrogen-on-demand applications because of their rapid reaction rates and stability under various conditions [33–35]. Independent experiments using commercially available $NaBH_4$ demonstrated that the catalyst can hydrolyze more than 99% of these solutions under the conditions of our experimental setup.

When the hydrogen release ceases, we assess the actual volume of hydrogen released against the theoretical volume, derived from the ideal gas law, that would have been obtained if all initial $NaBO_2 \cdot 4\,H_2O$ had converted to $NaBH_4$ (refer to Eq. (5)). This method enables the quantification of the chemical conversion yield without the need for additional separation steps, chemicals, or equipment. Although the accuracy may not reach the same level as separating with EDA, it offers a cleaner, cheaper, and simpler process sufficient to estimate the influence of the investigated operational variables. Furthermore, it facilitates the production of a "ready-to-use" solution, the half-life of which can be extended by further pH or temperature adjustments. Such a solution offers a new approach to storing regenerated $NaBH_4$ and streamlines parallel operations. Moreover, the low solubility of the remaining solids in the jar, namely MgO and $Mg(OH)_2$, allows for a simple and straightforward separation process via filtration.

2.5. Experimental cases definition: Fractional design of experiments

In this paper we investigate the simultaneous effects that varying molar ratio, BPR, milling time and rotational speed have on the mechanochemical conversion yield. In principle, the number of experimental cases n_{cases} is defined by Eq. (8).

$$n_{cases} = m^x \tag{8}$$

where m is the number of possible values (or levels) for each variable and x is the number of variables (or factors).

By defining three general levels for each of the four variables (high(2), medium(1) and low(0)) we can account for potential non-linear behavior and the total number of cases is 81. This number of experiments is prohibitive due to time, cost, and equipment availability constraints. As a result, we decided to employ a fractional design of experiments technique, namely screening, to reduce the number of cases needed to identify pertinent information about the main effects and two-factor interactions on the conversion yield [36].

As expected, this approach has some limitations. The most relevant is the risk of confounding, which binds together the effects of multiple factors, potentially leading to inaccurate conclusions about the true relationships between them. To minimize this risk, we select a resolution of the fourth (IV) degree reducing the total amount of experiments to 27. This configuration has no main effects confounded with interactions but at least one pair of two-variable interactions are confounded together [37]. To define the values for each level, it is important to define a wide and reasonable range [38]. For this, we use as reference both the operational limitations of our milling machine and the process parameters shown in Table 2. The levels for BPR (A) are defined as 10, 30 and 50. In the case of molar ratio (B), we use a molar ratio of 33%, 66% and 100% compared to the stoichiometric value for MgH_2. The milling time (C) is varied between 5, 12.5 and 20 h. Finally, the rotational speed (D) is set to 600, 800 and 1000 rpm. To ensure robustness, we applied randomization in the selection order of cases throughout the experimental process. Key cases with high conversion results were repeated twice to confirm reproducibility. The repeatability tests showed a maximum variation of 2.5%, which is significantly smaller than the variation observed between different parameter settings. Therefore, we do not include error bars in the interaction plots. The final screening design is shown in Table 3 which was created with Altair's HyperStudy v2022.1.

3. Results and discussion

In this section, the results of the experimental cases are presented and we leverage the screening design of experiments to assess the relevance of each of the studied operational variables: BPR (A), molar ratio (B), milling time (C), and rotational speed (D). Additionally, we evaluate the linear (L) and quadratic (Q) dependency of each operational variable to identify trends in yield performance. Then we assess specific cases of interest that are worth discussing in more detail. The conversion results, along with the linear and quadratic mapping, are presented in Table 4.

3.1. Analysis of variance (ANOVA)

The mapping presented in Table 4 was used to fit the models to assess the statistical significance of each variable, as well as to examine the dominance of linear versus quadratic effects. The linear mapping, denoted by 'L' for each factor (e.g., AL, BL), is derived directly from the treatment combination and follows this pattern: 0 is mapped to −1, 1 to 0, and 2 to 1. For instance, in case 9, where the treatment combination is defined as 0221, the mappings are as follows: AL is mapped to −1, BL and CL are mapped to 1, and DL is mapped to 0. The quadratic mapping, denoted by 'Q' (e.g., AQ, BQ), is then generated by squaring the linear values. However, this method results in identical values for zero, which is not ideal. To address this, we assign a value of −2 to the quadratic components corresponding to a linear value of 0 [39]. Returning to the example of case 9, AQ is calculated by squaring AL, resulting in 1, while BQ and CQ are also 1 after squaring their respective linear components. Finally, DQ is assigned a value of −2 because the corresponding linear component is 0.

Once the mapping is established, a full ANOVA model was fitted incorporating all factors and their interactions to assess their effect on the response variable. This analysis allows for the identification of significant factors and interactions, setting the stage for a more detailed examination of the individual contributions of linear and quadratic effects.

Subsequently, a separate ANOVA model was used to specifically evaluate the linear and quadratic components of each factor. This approach helped to clarify whether the relationship between the factors and the response variable was predominantly linear or quadratic. By comparing the results from both models, the most influential factors were identified, providing a deeper understanding of their impact on the response variable. A p-value is then employed as a metric to balance the risk between making type 1 errors (false positives) and type 2 errors (false negatives). Here, we opt for a cutoff p-value of 0.05 to determine statistical significance. The selection of this value means that there is a 5% chance of observing the obtained data if the null hypothesis is true (i.e., that the relevance of an operational variable does not affect the chemical yield). The results of the ANOVA are presented in Table 5.

The results presented in Table 5 indicate that the BPR, molar ratio, and milling time are statically significant in affecting the yield of the mechanochemical regeneration of $NaBH_4$. Additionally, the confounded two-factor interaction (AB,CD) between BPR/molar ratio and milling time/rotational speed also has statistical relevance. The ranking of these variables is effectively visualized with the Pareto plot in Fig. 3. In this Pareto plot, the F-value is used to rank the significance of each factor and interaction. The F-value quantifies the ratio of variance explained by a factor relative to the variance not explained by the model. A higher F value indicates a greater impact on the response variable.

The success in the mechanochemical yield has the strongest correlation with the milling time of the process. This is supported by the findings of previous studied as presented in Table 2 where it can be seen that high conversion yields necessitate long milling times. Moreover, while a proper individual selection of molar ratio and BPR is also significant for the success of the process, it is worth noting that they

Table 3
Screening design of experiments: experimental conditions.

Case	BPR (a)	Molar ratio (b)	Milling time [h] (c)	Rotational speed [rpm] (d)	Treatment combination
1	10	8	5	600	0000
2	10	8	12.5	800	0011
3	10	8	20	1000	0022
4	10	10	5	600	0100
5	10	10	12.5	1000	0112
6	10	10	20	600	0120
7	10	12	5	1000	0202
8	10	12	12.5	600	0210
9	10	12	20	800	0221
10	30	8	5	800	1001
11	30	8	12.5	1000	1012
12	30	8	20	600	1020
13	30	10	5	1000	1102
14	30	10	12.5	600	1110
15	30	10	20	800	1121
16	30	12	5	600	1200
17	30	12	12.5	800	1211
18	30	12	20	1000	1222
19	50	8	5	1000	2002
20	50	8	12.5	600	2010
21	50	8	20	800	2021
22	50	10	5	600	2100
23	50	10	12.5	800	2111
24	50	10	20	1000	2122
25	50	12	5	800	2201
26	50	12	12.5	1000	2212
27	50	12	20	600	2220

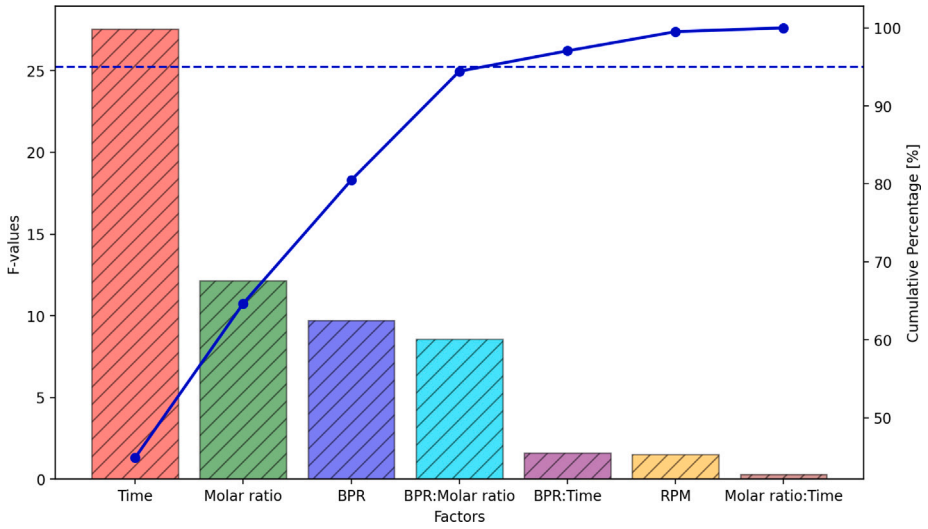

Fig. 3. Pareto plot of operational variables.

are affected by each other. As a consequence of this, their influence in the chemical conversion is leveled. This interaction has the risk of confounding with the two-factor interaction between milling time and rotational speed. However, our results suggest that rotational speed is not statistically significant in this study and thus, the risk of confounding is minimized. The lack of statistical significance of rotational speed is intriguing since previous studies consistently rely on high rotational speeds (>1000 rpm) to achieve high yields. Our findings suggest that this high energetic input is unnecessary as other operational variables will dominate the process. This result is compelling because it can decrease energy requirements and the wear experienced by the milling balls and jar during the process. Specifically, we observed that at higher rotational speeds (>1000 rpm) in the Emax, the material loss from the milling balls can become so significant that it contaminates the sample. One potential explanation is that the Emax can supply sufficient energy to regenerate $NaBH_4$ even at comparatively low rotational speeds. However, quantifying this is challenging with current state-of-the-art methods, as ball milling machines are often treated as black boxes. This is an area we plan to investigate further in future studies.

The results presented in Table 5 also provide a means to quantify linear and quadratic trends among individual factors. This is achieved by comparing the sum of squares between linear and quadratic terms. Specifically, the evolution of ball-to-powder ratio (BPR) and milling time is linearly explained, whereas the molar ratio is explained quadratically. This implies that there exists an optimal point for the molar ratio beyond which the chemical yield will be impacted negatively. This result is supported by the findings of Chen et al. [16] and can be visualized in the interaction plots presented in Fig. 4. These interaction plots are created by grouping the data based on two selected factors and plotting the average yield for each combination of their levels. Variables not plotted are averaged out, meaning their effects are integrated into the overall means, allowing the focus to be on the interaction between the plotted factors.

Interestingly, the quadratic dependency of the molar ratio tends to become linear as the second interacting factor decreases in level (A, C =

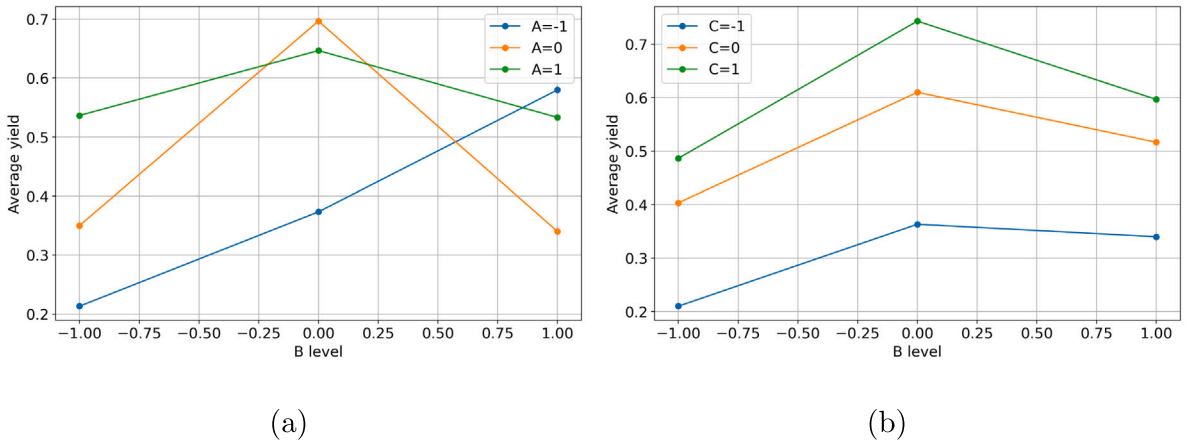

Fig. 4. (a) Interaction plot of BPR (A) and Molar ratio (B). (b) Interaction plot of Milling time (C) and Molar ratio (B). BPR levels: −1 = 10, 0 = 30, 1 = 50; Molar ratio levels: −1 = 33%, 0 = 66%, 1 = 100%; Milling time levels: −1 = 5 h, 0 = 12.5 h, 1 = 20 h.

Table 4
Conversion results for experimental cases. Linear and quadratic mapping.

Case	Treatment combination	Yield [%]	AL	AQ	BL	BQ	CL	CQ	DL	DQ
1	0000	12	−1	1	−1	1	−1	1	−1	1
2	0011	22	−1	1	−1	1	0	−2	0	−2
3	0022	30	−1	1	−1	1	1	1	1	1
4	0100	28	−1	1	0	−2	−1	1	−1	1
5	0112	39	−1	1	0	−2	0	−2	1	1
6	0120	45	−1	1	0	−2	1	1	−1	1
7	0202	40	−1	1	1	1	−1	1	1	1
8	0210	61	−1	1	1	1	0	−2	−1	1
9	0221	73	−1	1	1	1	1	1	0	−2
10	1001	26	0	−2	−1	1	−1	1	0	−2
11	1012	37	0	−2	−1	1	0	−2	1	1
12	1020	42	0	−2	−1	1	1	1	−1	1
13	1102	50	0	−2	0	−2	−1	1	1	1
14	1110	71	0	−2	0	−2	0	−2	−1	1
15	1121	88	0	−2	0	−2	1	1	0	−2
16	1200	21	0	−2	1	1	−1	1	−1	1
17	1211	32	0	−2	1	1	0	−2	0	−2
18	1222	49	0	−2	1	1	1	1	1	1
19	2002	25	1	1	−1	1	−1	1	1	1
20	2010	62	1	1	−1	1	0	−2	−1	1
21	2021	74	1	1	−1	1	1	1	0	−2
22	2100	31	1	1	0	−2	−1	1	−1	1
23	2111	73	1	1	0	−2	0	−2	0	−2
24	2122	90	1	1	0	−2	1	1	1	1
25	2201	41	1	1	1	1	−1	1	0	−2
26	2212	62	1	1	1	1	0	−2	1	1
27	2220	57	1	1	1	1	1	1	−1	1

Table 5
ANOVA.

Source of variation	Degrees of freedom	Sum of squares	p-value
A (BPR)	2	0.153	0.013
AL	1	0.151	–
AQ	1	0.002	–
B (Molar ratio)	2	0.191	0.007
BL	1	0.062	–
BQ	1	0.129	–
C (Milling time)	2	0.434	0.0009
CL	1	0.417	–
CQ	1	0.017	–
D (Rotational speed)	2	0.023	0.293
DL	1	0.003	–
DQ	1	0.020	–
AB,CD	6	0.270	0.011
AC,BD	6	0.050	0.286
AD,BC	6	0.009	0.874

–1). This behavior is observed in both interaction plots but the slope is considerably different. In the case of the low BPR, the increase in molar ratio results in higher yields, whereas in the case of low milling time, the increase in molar ratio leads to stagnation. The effect of milling time is straightforward to explain, as it is a critical variable in the process: longer milling times allow more opportunity for the quadratic dependency to exert influence, thus increasing yield. In contrast, the behavior with BPR presents a more intriguing phenomenon. The results suggest that the maximum yield shifts as BPR changes. Although the static nature of the selected levels prevents precise identification of these maxima, the trend indicates that a lower BPR requires a higher molar ratio to achieve maximum yield values. While this could potentially allow for the regeneration of more $NaBH_4$ in the same batch, it also implies an increased waste of material due to the need for a greater excess of MgH_2, which is undesirable.

The other statistically significant confounded interaction (C, D) milling time/ rotational speed may also be analyzed using the interaction plot shown in Fig. 5, even if rotational speed is not statistically significant as an individual factor.

As expected, longer milling times result in higher overall conversion yields, as shown by the green curve where C (milling time) = 1 (20 h). However, the same plot illustrates why rotational speed is not a significant variable for improving yield in this study. At each level of milling time, the highest average yield occurs at different rotational speeds, indicating that other variables are more influential in the process. It is worth highlighting that when shorter milling times are used (C = −1), the average yield increases linearly with higher rotational speeds, likely due to the increased number of collisions. However, the average yields for short milling times never reach those achieved with longer milling times (C = 0, 1). For these longer milling times, the average yields intersect, indicating that with sufficient milling time, other variables in the process become more influential and the correlation with rotational speed is lost. It is also notable that high rotational speeds (D = 1) lead to convergence of the average yield regardless of the remaining variables. This does not necessarily mean that maximum performance is achieved under these conditions, but it does help to standardize the results, effectively brute-forcing the conversion. This may explain why many of the results shown in Table 2 report high rotational speeds with little care for the remaining operational variables.

Lastly, it is important to highlight that the statistical significance of each individual factor and the corresponding two-factor interactions

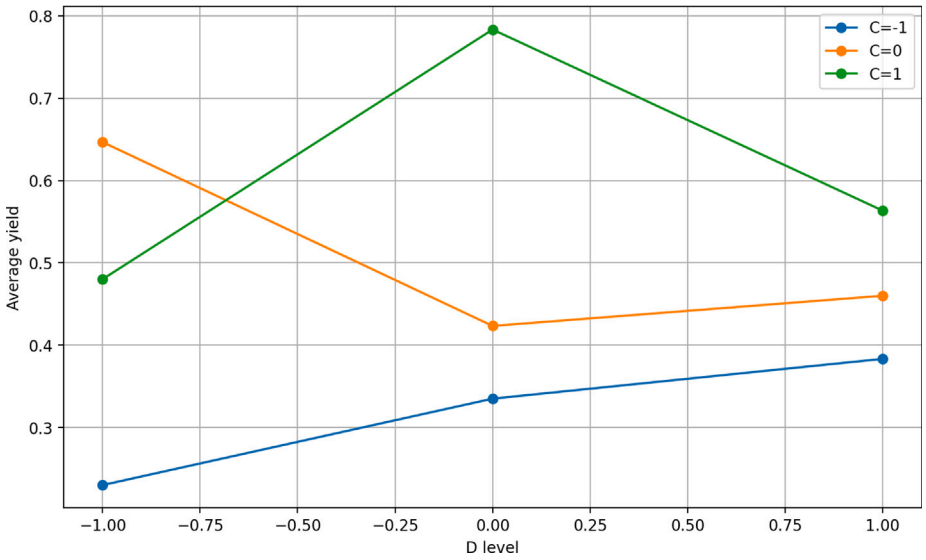

Fig. 5. Interaction plot of Milling time (C) and Rotational speed (D). Milling time levels: −1 = 5 h, 0 = 12.5 h, 1 = 20 h; Rotational speed levels: −1 = 600 rpm, 0 = 800 rpm. 1 = 1000 rpm.

are subject to the levels used in this study. We have explained the rationale behind the value selection for each level in Section 2.5. Naturally, for the sake of the discussion, had we selected a broader range in rotational speed, its statistical significance in the process could have increased.

3.2. Specific case analysis

The results in Table 4 show that case 24 achieves the highest conversion yield (90%) in this study. This outcome is obtained with a BPR of 50, an excess molar ratio of 66%, a milling time of 20 h, and a rotational speed of 1000 rpm. These conditions allow us to match the highest yield reported in the literature while reducing the rotational speed by 20% [16]. While this result is notable for achieving the same yield with lower energy requirements, it is also important to consider if other cases in this study, given the broad range of operational conditions, might be of interest.

The operating conditions of case 15 are particularly attractive as they achieve a regeneration yield of 88% while reducing the BPR by 40% and the rotational speed by an additional 20%. This supports our earlier observation that rotational speed does not statistically affect the conversion yield. Achieving nearly identical results with a reduced BPR demonstrates significant potential for optimizing the process conditions. This is also evident in Fig. 4(a). While a high BPR consistently yields high conversion rates regardless of the molar ratio, reducing the BPR requires more precise fine-tuning to maintain high yields, thus narrowing the range of high performance. Similar findings are reported in Table 2, where Çakanyıldırım et al. [13] achieved a 70% yield with a low BPR of 10. In other words, lenient operating conditions (e.g., high BPR, long milling times, and high rotational speed) facilitate achieving high conversion yields but are generally more costly and less efficient. Conversely, more stringent conditions reduce the range within which the mechanochemical process can obtain high conversion yields, but they offer performance benefits.

The previous observations clearly demonstrate the critical role of milling time in achieving high conversion yields, as both cases 15 and 24 required 20 h of operation. According to Fig. 4(b), while there is a noticeable difference in yields between processing times of 12.5 h and 20 h, the difference between 12.5 h and 5 h is much more significant. This is highlighted by cases 23 and 14, which achieve yields of 73% and 71%, respectively, with only 12.5 h of milling. Thus, reducing the milling time by 37.5%, from 20 to 12.5 h, results in only a 17% decrease in yield. This finding is economically significant and suggests that a shorter milling time could be advantageous. A detailed techno-economic analysis could be of interest to further explore this potential benefit.

Finally, cases 1–9, which use a BPR of 10, generally perform poorly, yielding low conversion rates that are not appealing. This performance only improves with a significant excess of MgH_2, which is not technically or economically attractive since the resulting MgO needs to be managed for a circular fuel cycle. Instead of using lower BPRs to process more material in the same batch at the expense of wasted material, it would be more advantageous to develop a larger machine that can replicate the mechanical conditions of the Emax. We plan to quantify these mechanical conditions in future research.

3.3. Iron contamination analysis

Given the highly abrasive environment inside the milling jar, it is relevant to estimate the expected levels of iron contamination resulting from the wear experienced by the milling balls. A straightforward method for estimating contamination levels involves weighing the milling balls before the milling process and after cleaning them. For this, we examine the wear experienced by the balls at rotational speeds of 1000 rpm and additionally, we implement 1200 rpm to serve as comparison benchmark. These tests were conducted with a milling time of 20 h and a BPR of 50, minimizing the amount of powder. Thus, this setup increases the potential percentage of impurities in the powder and reduces damping, resulting in more frequent and energetic collisions. Therefore, this approach allows us to examine the worst-case scenario.

As shown in Table 6, operating within the rotational speed range of 600–1000 rpm allows us to keep contamination levels below 6% even under the most abrasive conditions. If the milling time, BPR, or rotational speed are further reduced, contamination levels are expected to also decrease. This approximation does not account for contamination from the jar; however, we anticipate this to be minimal, as a layer of powder rapidly coats and protects the entire jar surface during the milling process.

4. Conclusions

We have conducted a comprehensive study on the importance of operational variables in the mechanochemical regeneration of $NaBH_4$,

Table 6
Fe-contamination calculations.

Ball size (mm)	Rotational speed (rpm)	Weight unused balls (g)	Weight used balls (g)	Percentage weight loss (%)	Total amount of wear (g)	Contamination percentage (%)
10	1200	97.06	96.73	0.34%	0.323	17%
10	1000	97.06	96.94	0.12%	0.117	6%

including ball-to-powder ratio, molar ratio, milling time, and rotational speed. Our results, covering a wide range of these variables, provide valuable insights for optimal selection and prioritization in future developments. Additionally, we introduced an inexpensive and straightforward method to quantify regeneration yield without additional chemicals, allowing the production of a 'ready-to-use' solution for on-demand hydrogen release.

Using a screening design of experiments, we investigated the influence of each operational variable on reaction yield. Our findings show that milling time is the most significant factor, followed by molar ratio and the interaction between molar ratio and ball-to-powder ratio. These results align with current state-of-the-art and offer insights into why previous studies selected specific conditions for high yields. We also found that rotational speed, often set at high values (i.e., >1000 rpm), does not significantly impact conversion yield compared to other variables. However, high rotational speeds homogenize yields, making them more consistent regardless of other conditions. While this does not ensure high yields, it results in yields converging toward an average value, which may explain their common use despite less optimization of other variables.

We reproduced the highest conversion yield reported using $NaBO_2 \cdot 4\,H_2O$ and MgH_2, with adjustments including a 20% reduction in rotational speed, offering energy savings. Given the wide range of conditions explored, we identified other attractive scenarios that, while not achieving the highest yields, offer economic advantages by processing more powder per batch or reducing milling time.

The ranking of operational variables holds within our experimental range. For instance, an extremely low rotational speed like 10 rpm would significantly reduce yield, despite being statistically insignificant in our analysis. This underscores the need for careful result interpretation and highlights substantial opportunities for optimization and future scale-up.

This work advances understanding of the complex interactions in the mechanochemical regeneration of $NaBH_4$. While we examined many variables, we believe the fill ratio, kept constant in this study, merits further exploration due to its potential impact on processing and yield. This will be investigated in future research. We hope our findings inspire further studies and contribute to more efficient and sustainable chemical processes.

CRediT authorship contribution statement

Santiago Garrido Nuñez: Writing – review & editing, Writing – original draft, Visualization, Validation, Software, Methodology, Investigation, Formal analysis, Data curation, Conceptualization. **Dingena L. Schott:** Writing – review & editing, Supervision, Methodology, Conceptualization. **Johan T. Padding:** Writing – review & editing, Validation, Supervision, Methodology, Investigation, Funding acquisition.

Funding

This work was supported by the project SH2IPDRIVE: Sustainable Hydrogen Integrated Propulsion Drives, funded by the RVO under grant MOB21013.

Declaration of competing interest

The authors declare the following financial interests/personal relationships which may be considered as potential competing interests: Johan T. Padding reports financial support was provided by Netherlands Enterprise Agency. If there are other authors, they declare that they have no known competing financial interests or personal relationships that could have appeared to influence the work reported in this paper.

References

[1] Bergthorson JM. Recyclable metal fuels for clean and compact zero-carbon power. Prog Energy Combust Sci 2018;68:169–96. http://dx.doi.org/10.1016/j.pecs.2018.05.001, URL http://www.sciencedirect.com/science/article/pii/S0360128518300327.

[2] van Rheenen E, Scheffers E, Zwaginga J, Visser K. Hazard identification of hydrogen-based alternative fuels onboard ships. Sustainability 2023;15(24). http://dx.doi.org/10.3390/su152416818, URL https://www.mdpi.com/2071-1050/15/24/16818.

[3] van Rheenen E, Padding J, Slootweg C, Visser K. A review of the potential of hydrogen carriers for zero emission, low signature ship propulsion systems. In: International naval engineering conference and exhibition. Online: Conference Proceedings of INEC; 2022-08-22, http://dx.doi.org/10.24868/10649.

[4] Crabtree GW, Dresselhaus MS, Buchanan MV. The hydrogen economy. Phys Today 2004;57(12):39–44. http://dx.doi.org/10.1063/1.1878333, arXiv:https://pubs.aip.org/physicstoday/article-pdf/57/12/39/9876773/39_1_online.pdf.

[5] Marrero-Alfonso EY, Beaird AM, Davis TA, Matthews MA. Hydrogen generation from chemical hydrides. Ind Eng Chem Res 2009;48(8):3703–12. http://dx.doi.org/10.1021/ie8016225, arXiv:https://doi.org/10.1021/ie8016225.

[6] Nunes HX, Silva DL, Rangel CM, Pinto AMFR. Rehydrogenation of sodium borates to close the NaBH4-H2 cycle: A review. Energies 2021;14(12). http://dx.doi.org/10.3390/en14123567, URL https://www.mdpi.com/1996-1073/14/12/3567.

[7] Abdelhamid HN. A review on hydrogen generation from the hydrolysis of sodium borohydride. Int J Hydrog Energy 2021;46(1):726–65. http://dx.doi.org/10.1016/j.ijhydene.2020.09.186, URL https://www.sciencedirect.com/science/article/pii/S0360319920336260.

[8] Tai T, Cao H, Feng W, Yin Z, Zhang H, Zheng G. High-efficient synthesis of NaBH4 by solid-phase electrolysis process on a core-shell-type cathode. Int J Hydrog Energy 2024;51:172–83. http://dx.doi.org/10.1016/j.ijhydene.2023.11.043, URL https://www.sciencedirect.com/science/article/pii/S0360319923057269.

[9] Urgnani J, Torres F, Palumbo M, Baricco M. Hydrogen release from solid state NaBH4. Int J Hydrog Energy 2008;33(12):3111–5. http://dx.doi.org/10.1016/j.ijhydene.2008.03.031, URL https://www.sciencedirect.com/science/article/pii/S0360319908003194, 2nd World Congress of Young Scientists on Hydrogen Energy Systems.

[10] Takacs L. What is unique about mechanochemical reactions? Acta Phys Pol A 2014;126:1040–3. http://dx.doi.org/10.12693/APhysPolA.126.1040.

[11] Hsueh C-L, Liu C-H, Chen B-H, Chen C-Y, Kuo Y-C, Hwang K-J, Ku J-R. Regeneration of spent-nabh 4 back to NaBH 4 by using high-energy ball milling. Int J Hydrog Energy - Int J Hydrog Energy 2009;34:1717–25. http://dx.doi.org/10.1016/j.ijhydene.2008.12.036.

[12] Kong L, Xinyu C, Jin H, Wu J, Du H, Xiong T. Mechanochemical synthesis of sodium borohydride by recycling sodium metaborate. Energy Fuels - Energy Fuel 2009;23. http://dx.doi.org/10.1021/ef900619y.

[13] Cakanyildirim C, Gürü M. Processing of NaBH4 from NaBO2 with MgH2 by ball milling and usage as hydrogen carrier. Renew Energy 2010;35:1895–9. http://dx.doi.org/10.1016/j.renene.2010.01.001.

[14] Lang C, Jia Y, Liu J, Wang H, Ouyang L, Zhu M, Yao X. NaBH 4 regeneration from NaBO 2 by high-energy ball milling and its plausible mechanism. Int J Hydrog Energy 2017;42. http://dx.doi.org/10.1016/j.ijhydene.2017.04.014.

[15] Ouyang L, Chen W, Liu J, Felderhoff M, Wang H, Zhu M. Enhancing the regeneration process of consumed NaBH 4 for hydrogen storage. Adv Energy Mater 2017;7:1700299. http://dx.doi.org/10.1002/aenm.201700299.

[16] Chen W, Ouyang L, Liu J, Yao X, Wang H, Liu Z, Zhu M. Hydrolysis and regeneration of sodium borohydride (NaBH 4) – a combination of hydrogen production and storage. J Power Sources 2017;359:400–7. http://dx.doi.org/10.1016/j.jpowsour.2017.05.075.

[17] Zhong H, Ouyang L, Ye J, Liu J, Wang H, Yao X, Zhu M. An one-step approach towards hydrogen production and storage. Energy Storage Mater 2017;7. http://dx.doi.org/10.1016/j.ensm.2017.03.001.
[18] Garrido Nuñez S, Schott DL, Padding JT. Predicting the energy dissipation in a high-energy ball mill with discrete element modeling. 2024, http://dx.doi.org/10.36227/techrxiv.172565505.54889130/v1.
[19] Tegel M, Schöne S, Kieback B, Röntzsch L. An efficient hydrolysis of MgH2-based materials. Int J Hydrog Energy 2017;42(4):2167–76. http://dx.doi.org/10.1016/j.ijhydene.2016.09.084, URL https://www.sciencedirect.com/science/article/pii/S0360319916327914.
[20] Grosjean M-H, Roué L. Hydrolysis of Mg–salt and MgH2–salt mixtures prepared by ball milling for hydrogen production. J Alloys Compd 2006;416(1):296–302. http://dx.doi.org/10.1016/j.jallcom.2005.09.008, URL https://www.sciencedirect.com/science/article/pii/S0925838805014118.
[21] Verbovytskyy YV, Berezovets VV, Kytsya AR, Zavaliy IY, Yartys VA. Hydrogen generation by the hydrolysis of MgH2. Mater Sci 2020;56(1):1–14. http://dx.doi.org/10.1007/s11003-020-00390-5.
[22] Chao CH, Jen TC. Reaction of magnesium hydride with water to produce hydrogen. In: Applied mechanics and materials. vol. 302, Trans Tech Publications, Ltd.; 2013, p. 151–7. http://dx.doi.org/10.4028/www.scientific.net/amm.302.151.
[23] Kreevoy MM, Jacobson RW. The rate of decomposition of NaBH4 in basic aqueous solutions. Ventron Alembic 1979;15:2–3.
[24] Retnamma R, Novais AQ, Rangel C. Kinetics of hydrolysis of sodium borohydride for hydrogen production in fuel cell applications: A review. Int J Hydrog Energy 2011;36(16):9772–90. http://dx.doi.org/10.1016/j.ijhydene.2011.04.223, URL https://www.sciencedirect.com/science/article/pii/S0360319911011220, European Fuel Cell 2009.
[25] Wang Q, Zhang LF, Zhao ZG. Hydrogen production by sodium borohydride in NaOH aqueous solution. IOP Conf Ser: Mater Sci Eng 2018;292(1):012031. http://dx.doi.org/10.1088/1757-899X/292/1/012031.
[26] Yahya MS, Ismail M. Synergistic catalytic effect of SrTiO 3 and Ni on the hydrogen storage properties of MgH 2. Int J Hydrog Energy 2018;43. http://dx.doi.org/10.1016/j.ijhydene.2018.02.028.
[27] Uesugi H, Sugiyama T, Nakatsugawa I, Ito T. Production of hydrogen storage material MgH2 and its application. J Japan Inst Light Met 2010;60:615–8, URL https://api.semanticscholar.org/CorpusID:13839396.
[28] Ismail M, Yahya MS, Sazelee N, Ali N, Yap F, Mustafa N. The effect of K2SiF6 on the MgH2 hydrogen storage properties. J Magn Alloys 2020;8. http://dx.doi.org/10.1016/j.jma.2020.04.002.
[29] Jen T-C, Adeniran J, Akinlabi E, Chao C-H, Ho Y-H, De Koker J. Hydrogen generation from acetic acid catalyzed magnesium hydride using an on-demand hydrogen reactor. 2016, http://dx.doi.org/10.1115/IMECE2016-66459, p. V06AT08A034.
[30] Huot J, Liang G, Boily S, Van Neste A, Schulz R. Structural study and hydrogen sorption kinetics of ball-milled magnesium hydride. J Alloys Compd 1999;293–295:495–500. http://dx.doi.org/10.1016/S0925-8388(99)00474-0, URL https://www.sciencedirect.com/science/article/pii/S0925838899004740.
[31] Durojaiye T, Hayes J, Goudy A. Rubidium hydride: An exceptional dehydrogenation catalyst for the lithium amide/magnesium hydride system. J Phys Chem C 2013;117(13):6554–60. http://dx.doi.org/10.1021/jp400961k, arXiv:https://doi.org/10.1021/jp400961k.
[32] Khan D, Zou J, Muhammad S, Khan NA, Saud S, Panda S. The adaptable effect of ru on hydrogen sorption characteristics of the MgH2 system. Mater Chem Phys 2023;301:127583. http://dx.doi.org/10.1016/j.matchemphys.2023.127583, URL https://www.sciencedirect.com/science/article/pii/S0254058423002912.
[33] Zou Y, Nie M, Huang Y, Wang J, Liu H. Kinetics of NaBH4 hydrolysis on carbon-supported ruthenium catalysts. Int J Hydrog Energy 2011;36(19):12343–51. http://dx.doi.org/10.1016/j.ijhydene.2011.06.138, URL https://www.sciencedirect.com/science/article/pii/S0360319911016107.
[34] Crisafulli C, Scirè S, Salanitri M, Zito R, Calamia S. Hydrogen production through NaBH4 hydrolysis over supported ru catalysts: An insight on the effect of the support and the ruthenium precursor. Int J Hydrog Energy 2011;36(6):3817–26. http://dx.doi.org/10.1016/j.ijhydene.2010.12.089, URL https://www.sciencedirect.com/science/article/pii/S0360319910024316, 3rd International Workshop in Hydrogen Energy.
[35] Zou Y, Huang Y, Li X, Liu H. A durable ruthenium catalyst for the NaBH4 hydrolysis. Int J Hydrog Energy 2011;36(7):4315–22. http://dx.doi.org/10.1016/j.ijhydene.2011.01.027, URL https://www.sciencedirect.com/science/article/pii/S0360319911000371, Emerging Materials Technology: Materials in Clean Power System.
[36] Yan Y, Helmons R, Wheeler C, Schott D. Optimization of a convex pattern surface for sliding wear reduction based on a definitive screening design and discrete element method. Powder Technol 2021;394:1094–110. http://dx.doi.org/10.1016/j.powtec.2021.09.041, URL https://www.sciencedirect.com/science/article/pii/S0032591021008342.
[37] Woods DC, Lewis SM. Design of experiments for screening. In: Ghanem R, Higdon D, Owhadi H, editors. Handbook of uncertainty quantification. Cham: Springer International Publishing; 2017, p. 1143–85. http://dx.doi.org/10.1007/978-3-319-12385-1_33.
[38] Montgomery DC. Design and analysis of experiments. 9th ed.. John Wiley & Sons; 2017.
[39] Dean A, Voss D, Draguljić D. Design and analysis of experiments. Springer International Publishing; 2017, http://dx.doi.org/10.1007/978-3-319-52250-0.